INSTITUTE OF PHYSICS PUBLISHING PLASMA SOURCES SCIENCE AND TECHNOLOGY

Plasma Sources Sci. Technol. **11** (2002) 97–103 PII: S0963-0252(02)32382-X

# Remote plasma-enhanced chemical vapour deposition of silicon nitride at atmospheric pressure

**G R Nowling, S E Babayan, V Jankovic and R F Hicks**

Chemical Engineering Department, University of California, Los Angeles, CA 90095, USA

E-mail: rhicks@ucla.edu

Received 26 October 2001, in final form 21 December 2001
Published 4 February 2002
Online at stacks.iop.org/PSST/11/97

**Abstract**

Silicon nitride films were deposited using an atmospheric pressure plasma source. The discharge was produced by flowing nitrogen and helium through two perforated metal electrodes that were driven by 13.56 MHz radio frequency power. Deposition occurred by mixing the plasma effluent with silane and directing the flow onto a rotating silicon wafer heated to between 100°C and 500°C. Film growth rates ranged from $90 \pm 10$ to $1300 \pm 130$ Å $\text{min}^{-1}$. Varying the $N_2/SiH_4$ feed ratio from 55.0 to 5.5 caused the film stochiometry to shift from $SiN_{1.45}$ to $SiN_{1.2}$. Minimum impurity concentrations of 0.04% carbon, 3.6% oxygen and 13.6% hydrogen were achieved at 500°C, and an $N_2/SiH_4$ feed ratio of 22.0. The growth rate increased with increasing silane and nitrogen partial pressures, but was invariant with respect to substrate temperature and rotational speed. The deposition rate also decreased sharply with distance from the plasma. These results combined with emission spectra taken of the afterglow suggest that gas-phase reactions between nitrogen atoms and silane play an important role in this process.

## 1. Introduction

Silicon nitride films play a significant role in ultra-large-scale integrated circuits. Due to their mechanical strength and resistance to sodium and moisture contamination, silicon nitride films are used as final encapsulation layers for fabricated devices [1–5]. They are excellent oxidation masks for recessed oxide processes and serve as diffusion barriers to dopants such as gallium [1–5]. Additionally, silicon nitride has been proposed for use in stacked gate dielectrics [3, 6–8].

Silicon nitride films may be deposited at low pressure using a variety of reactor configurations and process gas mixtures. In most plasma-enhanced chemical vapour deposition (PECVD) systems, the substrate is placed in direct contact with the plasma. This exposes the substrate to energetic ions and ultraviolet radiation, which may cause pinholes and electrically active defects to form in the film [9]. In remote PECVD, the substrate is placed downstream of the gas discharge and is not subject to damage. Furthermore, the silicon precursor gas mixes only with the plasma effluent. All remote processes are dominated by neutral chemistry and are thus easier to characterize and control [9–11]. Silicon nitride films are deposited using $NH_3$ and $N_2$ plasmas. $NH_3$ discharges produce fast growth rates and films with good conformality. However, the films typically contain 20–25 at.% hydrogen impurity, which is reduced to 6–15 at.% with the use of molecular nitrogen [1, 4, 9, 12–14].

Recently, there has been increased interest and development in plasma processes at atmospheric pressure [15–25]. Operating at reduced pressure requires vacuum chambers with load locks and robotic assemblies to shuttle materials in and out of vacuum. Consequently, the size of the objects that can be treated is limited by the size of the vacuum system. Atmospheric-pressure plasmas overcome this restriction. Moreover, they allow for continuous in-line processing of materials. At atmospheric pressure, remote PECVD proceeds exclusively via neutral chemistry. Over the past several years, new plasma sources have been developed which operate at atmospheric pressure, yet maintain the properties of low-pressure gas discharges [19–25]. The two most important

  

similarities are the generation of a high concentration of reactive species and a low neutral gas temperature (<200°C). With these devices, it is possible to explore the benefits of silicon nitride PECVD at atmospheric pressure.

In this paper, we provide the first example of the non-thermal, PECVD of silicon nitride at atmospheric pressure. A plasma source has been developed in which the feed gas flows through the electrodes and mixes with the precursor in the afterglow region. An advantage of this source is that the entire substrate may be contacted with the reactive gas mixture. Using nitrogen and silane as the precursors, we observe high deposition rates and good control over the film properties. The results indicate that gas-phase chemistry plays a key role in the process, and a preliminary reaction mechanism is proposed.

## 2. Experimental methods

A schematic of the atmospheric pressure plasma source is shown in figure 1. The plasma was maintained between two parallel electrodes made of anodized aluminium with a cross-sectional area of 11.4 $cm^2$. The electrodes were perforated, allowing inlet nitrogen and helium to flow through the plasma zone. The discharge was ignited and maintained by supplying 50 W RF power at 13.56 MHz to the top electrode. The bottom electrode was grounded and contained an internal network of channels through which silane was introduced. The silane exited through an isolated set of holes, mixing with nitrogen and helium only in the afterglow. A heated, spinning wafer stage was located downstream of the grounded electrode. The wafer backside temperature was measured by a thermocouple attached to the sample tray.

The silicon nitride films were deposited on n-type silicon (100) wafers, 2″ in diameter. Native oxides were removed prior to reaction by immersing the substrates in 10% hydrofluoric acid for 60 s. After loading the wafer into the reactor, the chamber was evacuated and filled with helium. Standard conditions were 769 Torr He (99.999%), 7.6 Torr $N_2$ (99.999%), 0.34 Torr $SiH_4$, a total flow rate of 40.8 l $min^{-1}$ (measured at 20°C and 1 atm), 50 W RF power (with negligible reflected power), a spin rate of 1000 rotations per minute (RPM), a wafer backside temperature of 450°C, and an wafer–electrode spacing of 7.6 mm. Before entering the discharge, the helium/nitrogen gas mixture was passed through an oxygen absorbing purifier (Matheson Gas Products, 6413). Although not utilized in this work, argon may have been used in place of helium with a RF power frequency of 27.12 MHz. Experiments were conducted by varying one parameter while keeping the others at their standard value. The ranges of the parameters investigated were 0–19 Torr $N_2$, 0–1.1 Torr $SiH_4$, a spin speed of 0–1400 RPM, a wafer temperature of 100–500°C, and an electrode–wafer spacing of 5.6–15.6 mm. As the RF power was increased from 50 to 62 W, the plasma arced, so the effect of RF power was not investigated in this study.

The samples were heated under a helium/nitrogen plasma, and upon reaching the desired backside temperature, the silane (5% $SiH_4$ in helium) was admitted to the reactor for 5.0 min. It was confirmed beforehand that the growth rate was constant from 0 to 12 min of operation. After reaction, the silane supply was shut off and the line purged with 2.4 ml $s^{-1}$ helium for 60 s before extinguishing the plasma. This was done to avoid exposing the wafer to any silane while cooling. It was verified that the precursor was removed quickly and no appreciable deposition occurred while purging the line. The system was then cooled in 8.0 l $min^{-1}$ flowing helium to 100°C before removing the wafer.

Optical emission from the $N_2$/He/$SiH_4$ afterglow was recorded using the apparatus shown in figure 2. Light from the plasma source was collected by a monochromator (Instruments S A, Triax 320) equipped with a 1200 groove $mm^{-1}$ grating blazed at 500 nm and a liquid nitrogen cooled CCD (Instruments S A, CCD-3000). The chamber was outfitted with windows that allowed transmission in the ultraviolet range. The signal was collected through a 1 mm pinhole via a quartz fibre-optic bundle connected to the monochromator. For these experiments only, the spinning wafer stage was replaced with a stationary stainless steel block, heated to a temperature of 450°C and positioned so as to minimize the recirculation of gas into the sampling area. The volume of gas sampled was 23.7 $mm^3$.

A nanospec (Nanometrics 210) was used to measure the film thickness. The values reported herein are the averages of 15 data points evenly spaced across the film. The deposition rate was determined by dividing the average film thickness by the reaction time. This measurement could be reproduced to within 90% in experiments repeated up to 10 separate times.

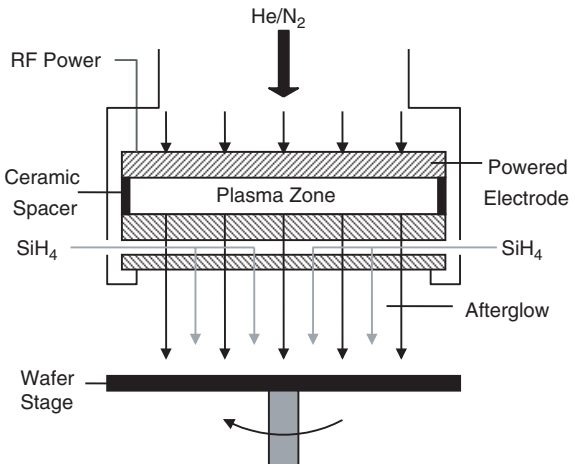


**Figure 1.** Schematic of the atmospheric-pressure plasma reactor.

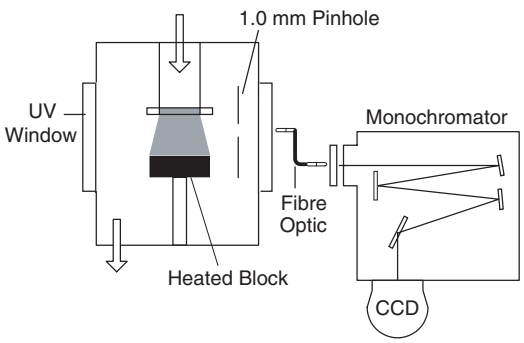


**Figure 2.** Schematic of the apparatus used to record the optical emission from the afterglow.

The film composition was examined by infrared spectroscopy using a Bio-Rad FTS-40A with a DTGS detector. Background reference scans of each wafer were taken before deposition and subtracted from scans of the film. The N/Si ratio in several films was determined using Rutherford backscattering spectroscopy (RBS). These experiments were performed using a 2.275 MeV $He^{++}$ ion beam, a probing area of 3.14 $mm^2$ and a backscattering angle of 160°. Also, secondary ion mass spectroscopy (SIMS) was used to determine the oxygen and carbon impurity concentrations. This was done using a $Cs^+$ ion beam and a PHI 6600 Quadrupole SIMS machine. Finally, the stress of several films was measured using a Tencor FLX-2320A system.

## 3. Results

### *3.1. Gas-phase chemistry*

A photograph of the afterglow of the atmospheric pressure helium–nitrogen discharge is presented in figure 3(*a*). Whereas in figure 3(*b*), a picture is shown of the discharge under the same conditions, but with silane added to the afterglow. The orange emission seen in figure 3(*a*) is due to the relaxation of $N_2(B^3\Pi_g)$ molecules [26–28]. It appears long-lived in the afterglow due to its continual production via the three-body recombination of ground-state nitrogen atoms [29–31]:

$$N + N + M \rightarrow N_2(B^3\Pi_g) + M \qquad (1)$$

The observation of $N_2(B)$ indicates that there is a high concentration of ground-state nitrogen atoms extending to more than 80 mm below the bottom electrode. However, upon addition of silane, the $N_2(B)$ emission is largely extinguished, and a new violet emission arises due to SiH ($A^2\Delta$–$X^2\Pi$) and SiN ($A^2\Sigma$–$X^2\Sigma$) transitions [28, 32].

The above observations are confirmed via optical spectroscopy of the gas. The scans were taken at a distance of $4.0 \pm 0.5$ mm downstream of the bottom electrode. In figure 4, the $N_2(B,\nu = 4\text{–}9)$ emission spectrum is shown before and after silane introduction [28]. The total peak area is reduced by 93% after adding $SiH_4$. Figure 5 shows several emission peaks that are characteristic of the He/$N_2$/$SiH_4$ afterglow. The SiH and SiN bands in the 400–430 nm range are responsible for the violet colour of the afterglow [28, 32]. The single peak at 336–338 nm is due to NH ($A^3\Pi$–$X^3\Sigma^-$) emission [28, 32]. The consumption of nitrogen atoms combined with the appearance of new species indicates that gas-phase reactions between the nitrogen atoms and silane occur during silicon nitride PECVD in this reactor.

### *3.2. Deposition rate trends*

The effect of the $N_2$ and $SiH_4$ partial pressures on the growth rate is shown in figure 6. The rate increases with nitrogen partial pressure. Based on the slope of the log–log plot, the reaction order in nitrogen is 0.5. The maximum nitrogen partial pressure that can be fed to the plasma is 19 Torr. Above this amount, the plasma becomes unstable and arcs. The deposition rate also increases with $SiH_4$ partial pressure, but to a lesser extent. The reaction order is only 0.1 in the range of 0.07–2.0 Torr $SiH_4$. Below 0.07 Torr, the rate falls off quickly. Finally, when either the silane or nitrogen partial pressure is set to zero, no film growth occurs.

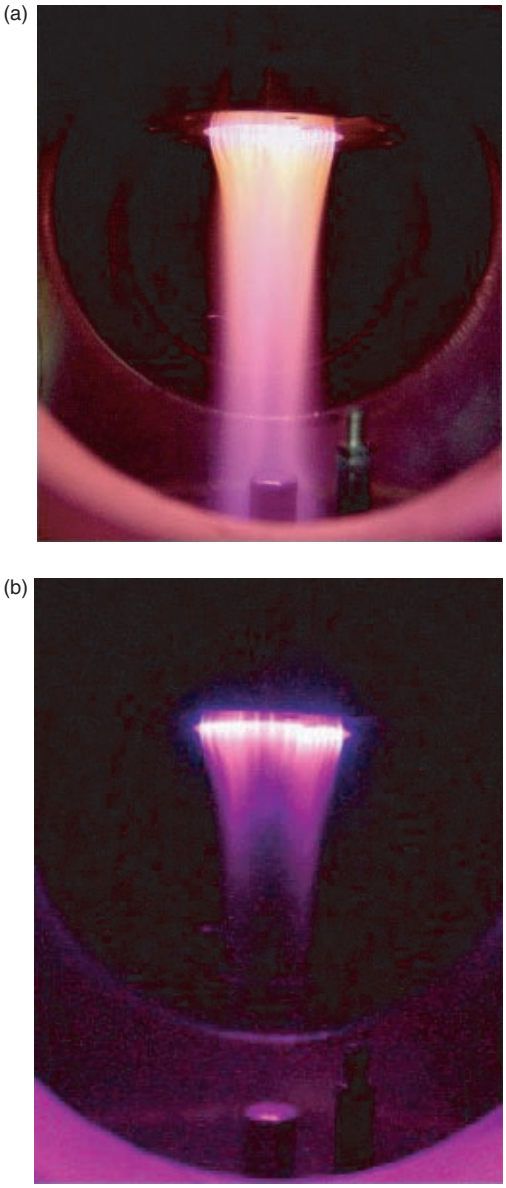


**Figure 3.** Photograph of the (*a*) He/$N_2$ afterglow and (*b*) He/$N_2$ afterglow mixed with silane. The conditions were 769 Torr He, 7.6 Torr $N_2$, 0.17 Torr $SiH_4$, and 50 RW power.

In figure 7, the deposition rate is plotted against the wafer backside temperature. No dependence is observed from 100°C to 500°C. The average rate equals $525 \pm 42$ Å $min^{-1}$.

Shown in figure 8 is the dependence of the film growth rate on the electrode–wafer spacing. The rate is strongly affected by the distance the gas must travel prior to encountering the wafer. The rate falls by 91% upon increasing the spacing from 5.6 to 13.6 mm, with no deposition observed at or beyond 15.6 mm.

In addition to these results, it has been determined that the growth rate is invariant with respect to spin rate for speeds varying from 100 to 1400 RPM. A maximum rate of 1300 Å $min^{-1}$ is obtained at 18 Torr $N_2$, 1.1 Torr $SiH_4$, an electrode–wafer spacing of 5.6 mm, and all other variables at the standard conditions.

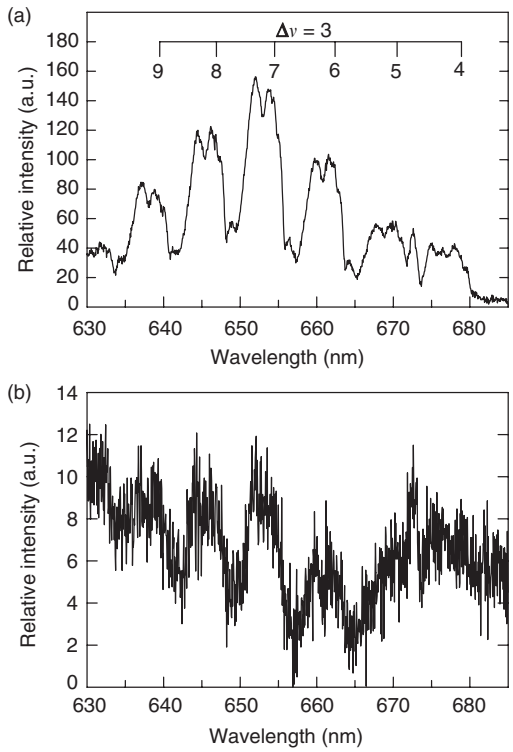


**Figure 4.** Spectra taken of $N_2$(B) emission in the afterglow (*a*) before and (*b*) after adding silane.

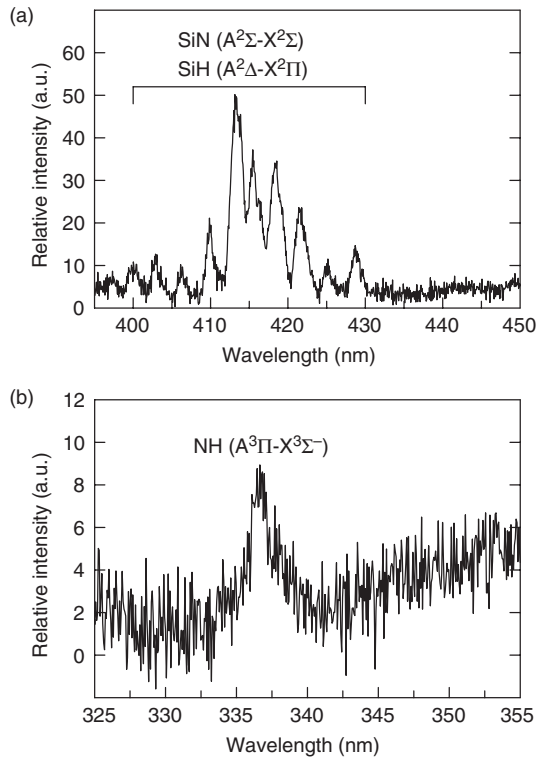


**Figure 5.** Emission spectra of electronically excited intermediates observed in the He/$N_2$ afterglow after $SiH_4$ addition [28].

### *3.3. Film composition*

We have found that the film composition depends on the nitrogen partial pressure. Stoichiometric silicon nitride, $Si_3N_4$, has an N/Si ratio of 1.33 [3]. Films deposited at 19.0 Torr $N_2$ are slightly nitrogen rich with N/Si = 1.45 (as determined by RBS), while films deposited at 1.9 Torr $N_2$ are silicon rich with N/Si = 1.22. It is estimated that films grown at approximately 10 Torr $N_2$ should be stoichiometric. Although the deposition rate is insensitive to temperature, this variable does affect the film composition. Films deposited at 200°C have impurity concentrations of 0.15 at.% carbon and 6.3 at.% oxygen. At 500°C, the concentrations are reduced to 0.04 at.% carbon and 3.6 at.% oxygen. The sources of these impurities are most likely traces of oxygen and carbon in the process gas and chamber walls.

Presented in figure 9 are infrared absorption spectra of films grown at 100°C, 300°C and 500°C. The primary bands

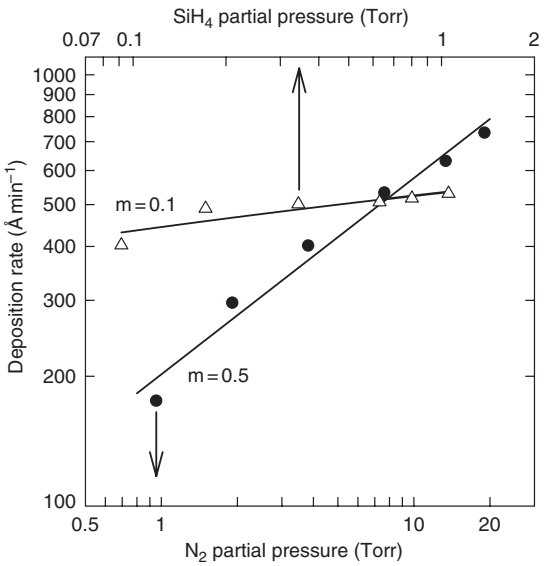


**Figure 6.** The dependence of the deposition rate on the nitrogen and silane partial pressures at 769 Torr He, 50 W RF power, 1000 RPM, 450°C, an electrode–wafer spacing of 7.6 mm, 0.34 Torr $SiH_4$, and 7.6 Torr $N_2$ unless otherwise noted.

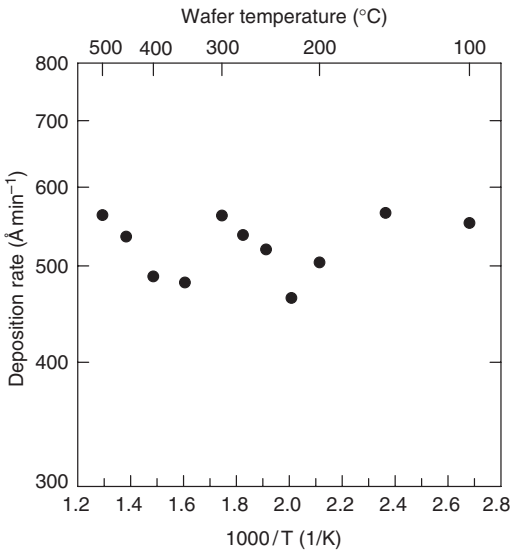


**Figure 7.** The dependence of the deposition rate on the substrate temperature at 769 Torr He, 7.6 Torr $N_2$, 0.34 Torr $SiH_4$, 50 W RF power, 1000 RPM, and an electrode–wafer spacing of 7.6 mm.

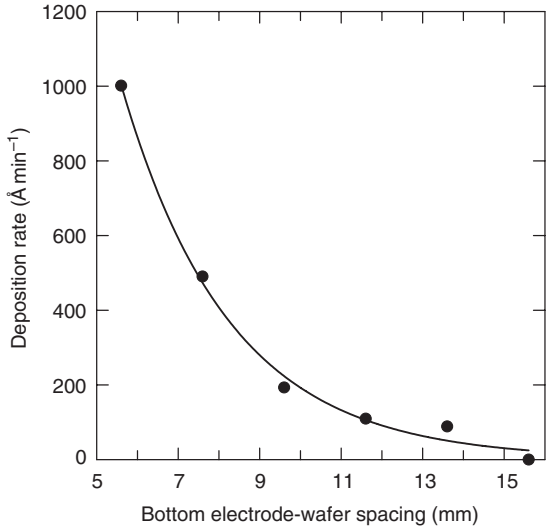


**Figure 8.** The dependence of the deposition rate on the electrode–wafer spacing at 769 Torr He, 7.6 Torr $N_2$, 0.34 Torr $SiH_4$, 50 W RF power, 450˚C and 1000 RPM.

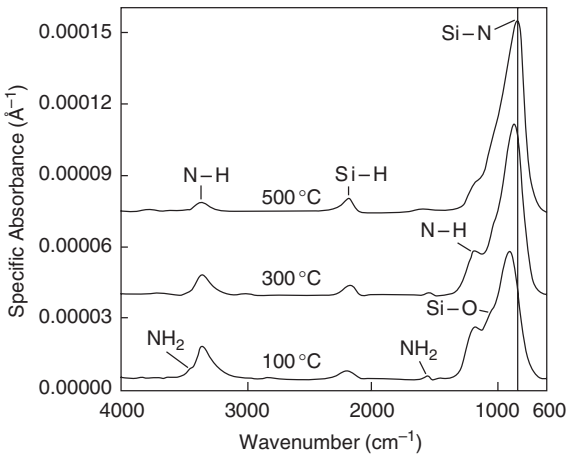


**Figure 9.** Infrared spectra of the silicon nitride films deposited at substrate temperatures of 100˚C, 300˚C and 500˚C.

of interest are the Si–N, Si–H, and N–H stretching vibrations at 835, 2150, and 3345 $cm^{-1}$, respectively [1, 9, 11, 13, 33]. A small peak at 1550 $cm^{-1}$ and a shoulder at 3460 $cm^{-1}$ are due to $NH_2$ stretching and bending modes [13, 34], while the shoulder at 1080 $cm^{-1}$ results from an Si–O stretching mode [1, 25]. As the temperature increases, one sees a decrease in the NH, $NH_2$, and SiO vibrational bands, but no change in the Si–H peak intensity. Another point of interest is a shift in the Si–N peak to lower wave numbers. This is a consequence of reducing the N–H and oxygen content in the film [11, 35].

The total hydrogen concentration and its bonding configurations have been estimated from the integrated peak areas and the absorption coefficients determined by Lanford and Rand [36]. At 100˚C, the film has a total hydrogen content of 37.5 at.% with 90% of the H atoms bonded to nitrogen. At 500˚C, the total hydrogen content is reduced to 13.9 at.% with 65% of the H atoms bonded to nitrogen.

The hydrogen concentration and its bonding sites depend on the inlet gas composition as well. In figure 10, we illustrate how the amount of hydrogen and its partitioning between

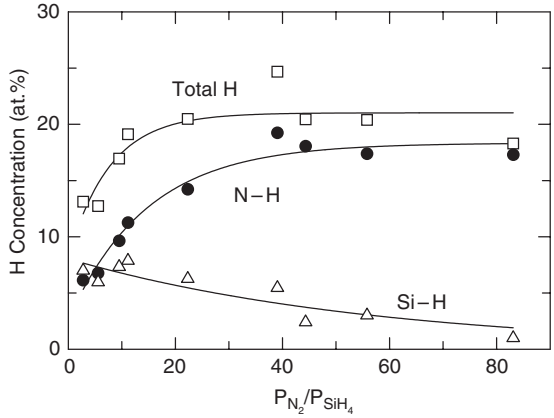


**Figure 10.** The effect of the $N_2/SiH_4$ partial pressure ratio on the total hydrogen concentration in the film and its partitioning between N and Si.

nitrogen and silicon varies with $N_2/SiH_4$ partial pressure ratio. At low ratios, the total hydrogen content is roughly 13 at.% and is distributed equally between the Si and N. As the nitrogen partial pressure increases, more hydrogen atoms are attached to the nitrogen, while the amount of silicon–hydrogen bonds gradually decreases. At the maximum $N_2/SiH_4$ ratio of 84, the total hydrogen content is roughly 20 at.%, with 85% of the H atoms bonded to nitrogen.

## 4. Discussion

The results presented above indicate that high quality silicon nitride can be deposited by remote PECVD at atmospheric pressure. By varying the nitrogren partial pressure, it is possible to grow films that are either nitrogen rich, silicon rich, or stoichiometric. By increasing the substrate temperature to 500˚C, oxygen, carbon, and hydrogen impurity levels can be lowered to 3.6, 0.04, and 13.6 at.%, respectively. One may further reduce the hydrogen content at 500˚C by dropping the $N_2/SiH_4$ ratio from 22 down to about 13. Although not studied in depth, the films have been found to be under tensile stress, on the order of 700 MPa.

The results obtained on the film stoichiometry are similar to that seen in low-pressure PECVD reactors. In these systems, film compositions can be pushed to either side of the value in the crystalline material by changing the ratio of nitrogen and silane in the feed [33, 37]. This is consistent with our RBS data of films deposited at high and low nitrogen partial pressures.

The tensile stress exhibited by our films is the opposite of what one obtains from low-pressure PECVD systems [1, 3, 4, 38]. In the latter reactors, ion bombardment plays a key role in causing the films to be under compressive stress. Even material grown in low-pressure, remote plasma reactors exhibit compressive stresses due to the penetration of ions into the afterglow [1, 37, 39]. In the atmospheric-pressure plasma discharge examined in this study, charged species are insignificant in the afterglow, since their concentration quickly drops from about $10^{11}$ to $<10^9$ $cm^{-3}$ in a few $\mu$s [19, 26, 27, 40]. Evidently, for this reason, the silicon nitride films are under tensile stress.

While our minimum hydrogen content is on par with films deposited at low pressure, the bonding arrangements

are not typical. With low-pressure $N_2/SiH_4$ systems, the majority of hydrogen is bonded to silicon and, in many cases, there is no detectable N–H bonding [9, 12, 13]. As shown in figures 9 and 10, decreasing the temperature, or increasing the $N_2/SiH_4$ ratio, causes the hydrogen to be bonded almost exclusively to nitrogen. This dominance of N–H bonding is more characteristic of films produced in reactors using ammonia and silane reagents [12–14]. In the latter case, ammonia is the primary source of the hydrogen impurity, and high substrate temperatures are essential for minimizing this phenomenon [4, 13, 14]. Note that the same trend in N–H concentration with temperature is displayed in figure 9.

The growth rates measured in this study span a range of 90–1300 Å, and are strongly dependent on the operating parameters. The electrode–wafer spacing has the largest effect on the rate. Increasing the gap by 8 mm decreases the rate by 91%. In addition, the deposition rate rises with nitrogen partial pressure, exhibiting a reaction order of 0.5 in $N_2$. The effect of silane is less significant, with a reaction order of only 0.1 in $SiH_4$. Without adding either nitrogen or silane to the plasma, no deposit is detected on the silicon wafer.

For the most part, the above trends are followed in remote, low-pressure, $N_2/SiH_4$ plasmas. Theil *et al* [12] observed a decrease in the deposition rate as the wafer was moved further from the discharge. However, the drop was only 60–70% over a spacing of 9 cm. Obviously, the effect of spacing is far more pronounced at atmospheric pressure. In low-pressure processes, the growth rate also increases with increasing $SiH_4$ and $N_2$ partial pressures [37, 39, 41]. There is disagreement though with regard to the effect of substrate temperature, since in some studies the growth rate declines with temperature [9, 41].

Recently, there have been several studies of remote PECVD systems utilizing electron cyclotron resonance plasmas [1, 14, 33, 37, 39]. The high density of charged species allows the silicon nitride films to be formed at temperatures as low as 50°C. These reactors typically yield growth rates in the range of 500–600 Å $min^{-1}$ [37, 39]. By comparison, our atmospheric-pressure plasma deposits silicon nitride films of the same quality at double the rate. In addition, the maximum rate is substantially higher than that achieved in microwave plasmas, which is ∼1100 Å $min^{-1}$ [41].

By considering the data presented thus far, it is possible to propose a mechanism for the PECVD process. The rate data shows that nitrogen species generated in the plasma drive the reaction. The emission spectra, deposition rate behaviour, and film composition further indicate that gas-phase reactions occur between the active nitrogen species and silane.

Babayan *et al* [26, 27] have characterized the chemical composition of an atmospheric-pressure plasma containing nitrogen and helium and with similar discharge characteristics. There are four active species of interest: ground-state atomic nitrogen $N(^4S)$, and three excited states of molecular nitrogen, $N_2(A^3\Sigma_u)$, $N_2(B^3\Pi_g)$, and $N_2(C^3\Pi_u)$. The concentrations generated by the plasma in this study are as follows: $4.8 \times 10^{15}$ $cm^{-3}$ of N, $2.1 \times 10^{13}$ $cm^{-3}$ of $N_2(A)$, $1.2 \times 10^{12}$ $cm^{-3}$ of $N_2(B)$, and $3.2 \times 10^9$ $cm^{-3}$ of $N_2(C)$. The nitrogen atom density is $10^2$–$10^5$ times that of the other active species. Furthermore, its high concentration persists for several centimetres in the afterglow [26, 27]. This results from the fact that the three-body recombination of nitrogen atoms is slow compared to the collisional relaxation pathways available to the molecular nitrogen species [26, 27, 42–44]. A density of $\sim 5.0 \times 10^{15}$ $cm^{-3}$ N atoms produces an $N_2(B)$ density of $\sim 8.0 \times 10^9$ $cm^{-3}$ via equation (1) above, which explains the intense pink-orange glow seen in the picture presented in figure 3(*a*).

As shown in figures 3–5, the afterglow emission changes dramatically upon introducing the silane feed. This is a clear indication that nitrogen atoms are consumed by reaction with $SiH_4$, yielding $SiH_x$, $SiN_y$, and $NH_z$ species. It is proposed that the gas-phase initiation step is

$$N + SiH_4 \rightarrow NH + SiH_3 \tag{2}$$

Piper *et al* [32] have measured the rate constant of this reaction as well as that between $SiH_4$and $N_2(A)$. The rate constant with $N_2(A)$ is higher than that with atomic nitrogen. Nevertheless, in the atmospheric pressure afterglow, the density of N atoms is several orders of magnitude higher than that of $N_2(A)$, making equation (2) the most likely initiation pathway.

Further evidence for gas-phase chemistry comes from the film composition results. As explained at the beginning of this section, many of the film properties are not typical of those obtained from low-pressure plasmas fed with $N_2$ and $SiH_4$. Instead, they display properties characteristic of PECVD processes using $NH_3$ and $SiH_4$. In these latter systems, $NH_x$ fragments are the key species that react with the silane to drive deposition [10, 13, 14]. This suggests that in the afterglow of our atmospheric-pressure plasma, a significant number of the nitrogen atoms are converted to $NH_x$ species prior to striking the substrate. After initiation, gas-phase propagation reactions will produce $NH_x$ radicals as follows:

$$N + SiH_x \rightarrow NH + SiH_{x-1} \tag{3}$$

where $x$ equals 1, 2, or 3. An additional propagation step that would produce the observed SiN radical is

$$N + SiH \rightarrow SiN + H \tag{4}$$

There are two possible explanations for the observed drop in growth rate with distance. On the one hand, nitrogen atoms may be required to adsorb on the surface along with $SiH_x$ radicals. These N atoms would abstract H atoms from the $SiH_x$ radicals, causing the reaction to proceed. As the wafer is spaced further away, more N atoms are consumed in the gas, thus inhibiting deposition. In the second possibility, the $NH_x$ radicals are required to adsorb onto the film surface and react with the $SiH_x$ radicals to form silicon nitride. Here, the $NH_x$ species are deactivated by collision with silane or hydrogen in the gas, with formation of $NH_3$. For example [10]:

$$NH_2 + SiH_4 \rightarrow NH_3 + SiH_3 \tag{5}$$

or

$$NH_2 + H + M \rightarrow NH_3 + M \tag{6}$$

In either case, any $NH_x$ fragment that reacts to from $NH_3$ cannot deposit, since the substrate temperature is insufficient to promote $NH_3$ dissociation. Further work is underway to determine which of the above two pathways dominates the atmospheric-pressure PECVD of silicon nitride.

Prior work at low pressures has led to some discrepancies regarding the importance of gas-phase chemistry. Several

authors have suggested that nitrogen atoms dissociate silane, producing $NH_x$ and $SiH_x$ radicals [32, 45–47]. These can further combine with themselves or other nitrogen species to produce gaseous $SiN_xH_y$ species. By contrast, other researchers argue against silane dissociation, and instead claim there is little gas-phase chemistry in either remote or direct plasma reactors containing nitrogen and silane [10, 41, 48, 49]. These authors believe that film deposition occurs exclusively via a heterogeneous reaction mechanism involving adsorbed silane and activated nitrogen. At least in the atmospheric-pressure PECVD process described here, reactions do occur in the gas and influence the growth rate and film properties. One consequence of this chemistry is the consumption of the reactive intermediates responsible for film deposition.

## 5. Conclusions

We have demonstrated the PECVD of high quality silicon nitride films at one atmosphere pressure. The film composition is strongly dependent on the process conditions and varies on either side of the $Si_3N_4$ stoichiometry, depending on the $N_2/SiH_4$ inlet ratio and substrate temperature. The deposition rates are 2–3 times higher than those recorded in low-pressure, remote PECVD systems. The growth rate strongly depends on the electrode–wafer spacing, but is independent of temperature. We conclude that gas-phase reactions involving ground-state nitrogen atoms and silane play an important role in the reaction mechanism.

## Acknowledgments

This work was supported by the National Science Foundation, Division of Chemical and Transport Systems; the UC-SMART program; and AMD.

## References

[1] Yota J, Handler J and Saleh A A 2000 *J. Vac. Sci. Technol.* A **18** 372
[2] Basa D K, Bose M and Bose D N 2000 *J. Appl. Phys.* **87** 4324
[3] Jaeger R C 1993 *Modular Series on Solid State Devices, Vol. 5: Introduction to Microelectronic Fabrication* (Reading, MA: Addison-Wesley)
[4] Lieberman M A and Lichtenberg A J 1994 *Principles of Plasma Discharges and Materials Processing* (New York: Wiley-Interscience)
[5] Sze S M 1985 *Semiconductor Devices* (New York: Wiley)
[6] Landheer D, Ma P, Lennard W N, Mitchell I V and McNorgan C 2000 *J. Vac. Sci. Tecnol.* A **18** 2503
[7] Lucovsky G, Wu Y, Niimi H, Yang H, Keister J and Rowe J E 2000 *J. Vac. Sci. Technol.* A **18** 1163
[8] Lucovsky G, Niimi H, Wu Y, Parker R and Hauser J R 1998 *J. Vac. Sci. Technol.* A **16** 1721
[9] Alexandrov S E, Hitchman M L and Shamlian S 1993 *Adv. Mater. Optics Electronics* **2** 301
[10] Kushner M J 1992 *J. Appl. Phys.* **71** 4173
[11] Lucovsky G and Tsu D V 1987 *J. Vac. Sci. Technol.* A **5** 2231
[12] Theil J A, Hattangady S V and Lucovsky G 1992 *J. Vac. Sci. Technol.* A **10** 719
[13] Lucovsky G, Richard P D, Tsu D V, Lin S Y and Markunas R J 1986 *J. Vac. Sci. Technol.* A **4** 682
[14] Kotecki D E and Chapple-Sokol J D 1995 *J. Appl. Phys.* **77** 1284
[15] Fauchais P and Vardelle A 1997 *IEEE Trans. Plasma Sci.* **25** 1258
[16] Smith R W, Wei D and Apelian D 1989 *Plasma Chem. Plasma Process.* **9** 135S
[17] Goldman M and Sigmond R S 1982 *IEEE Trans. Elec. Insul.* **EI-17**
[18] Eliasson B and Kogelschatz U 1991 *IEEE Trans. Plasma Sci.* **19** 1063
[19] Schütze A, Jeong J Y, Babayan S E, Park J, Selwyn G S and Hicks R F 1998 *IEEE Trans. Plasma Sci.* **26** 1685
[20] Jeong J Y, Babayan S E, Tu V J, Henins I, Velarde J, Selwyn G S and Hicks R F 1998 *Plasma Sources Sci. and Tech.* **7** 282
[21] Babayan S E, Jeong J Y, Tu V J, Selwyn G S and Hicks R F 1998 *Plasma Sources Sci. and Tech.* **7** 286
[22] Jeong J Y, Babayan S E, Schütze A, Tu V J, Park J, Henins I, Selwyn G S and Hicks R F 1999 *J. Vac. Sci. Technol.* A **17** 2581
[23] Jeong J Y, Park J, Henins I, Babayan S E, Tu V J, Selwyn G S, Ding G and Hicks R F 2000 *J. Phys. Chem.* **104** 8027
[24] Tu V J, Jeong J Y, Schütze A, Babayan S E, Selwyn G S, Ding G and Hicks R F 2000 *J. Vac. Sci. Technol.* A **18** 2799
[25] Babayan S E, Jeong J Y, Schütze A, Tu V J, Moravej M, Selwyn G S and Hicks R F 2001 *Plasma. Sources. Sci. Technol.* **10** 573
[26] Babayan S E, Ding G and Hicks R F 2001 *Plasma Chem. Plasma Process.* **21** 505
[27] Babayan S E, Ding G, Nowling G R, Yang X and Hicks R F 2001 *Plasma Chem. Plasma Process.* (in press)
[28] Pearse R W B and Gaydon A G 1979 *The Identification of Molecular Spectra* (New York: Chapman and Hall)
[29] Ricard A, Tetreault J and Hubert J 1991 *J. Phys. B: At. Mol. Phys.* **24** 1115
[30] Noxon J F 1962 J. Chem. Phys. **36** 926
[31] Campbell I M and Thrush B A 1967 *Proc. Roy. Soc.* A **296** 201
[32] Piper L G and Caledonia G E 1991 *J. Phys. Chem.* **95** 698
[33] Bae S, Farber D G and Fonash S J 2000 *Solid-State Electronics* **44** 1355
[34] Hanyaloglu B F and Aydil E S 1998 *J. Vac. Sci. Technol.* A **16** 2794
[35] Budhani R C, Prakash S, Doerr H J and Bunshah R F 1987 *J. Vac. Sci. Technol.* A **5** 1644
[36] Lanford W A and Rand M J 1978 *J. Appl. Phys.* **49** 2473
[37] Doughty C, Knick D C, Bailey J B and Spencer J E 1999 *J. Vac. Sci. Technol.* A **17** 2612
[38] Wolf S and Tauber R N 1986 *Silicon Processing for the VLSI Era Vol 1: Process Technology* (Sunset Beach, CA: Lattice)
[39] Leclerc S, Lecours A, Carson M, Richard E, Turcotte G and Currie J F 1998 *J. Vac. Sci. Technol.* A **16** 881
[40] Guerra V and Loureiro J 1997 *Plasma Sources Sci. Technol.* **6** 361
[41] Landheer D, Skinner N G and Jackman T E 1991 *J. Vac. Sci. Technol.* A **9** 2594
[42] Herron J T 1999 *J. Phys. Chem. Ref. Data* **28** 1453
[43] Ionikh Y Z and Chernysheva N V 1990 *Opt. Spectrosc. (USSR)* **68** 598
[44] Gat E, Gherardi N, Lemoing S, Massines F and Ricard A 1999 *Chem. Phys. Lett.* **306** 263
[45] Meikle S and Hatanaka Y 1990 *Appl. Phys. Lett.* **57** 762
[46] Auberton J, Conte D, Jauberteau J L and Jauberteau I J 2000 *J. Phys. D: Appl. Phys.* **33** 1499
[47] Jaubertau J L, Conte D, Baraton M I, Quintard P, Auberton J and Catherinot A 1990 *Plasma Chem. Plasma Process.* **10** 401
[48] Smith D L, Alimoda A S and von Presissig F J 1990 *J. Vac. Sci. Technol.* B **8** 551
[49] Smith D L 1993 *J. Vac. Sci. Technol.* A **11** 1843